IIETA International Information and Engineering Technology Association
Advancing the World of Information and Engineering

Revue des Composites et des Matériaux Avancés-Journal of Composite and Advanced Materials
Vol. 36, No. 2, April, 2026, pp. 319-333
Journal homepage: http://iieta.org/journals/rcma

Multi-Objective Optimization of E-Glass/S-Glass and HS-Carbon Hybrid Laminates with Holes for Improved Torsional Performance

Ibrahim Beroual[1*], Moussa Amadji[2,3]

[1] Laboratory of Mechanics, Structures and Energetics (LMSE), Department of Mechanical Engineering, Faculty of Construction Engineering, Mouloud Mammeri University, Tizi-Ouzou 15000, Algeria
[2] Institute of Industrial Hygiene and Safety, University of Chahid Mostefa Ben Boulaïd - Batna 2, Batna 05000, Algeria
[3] Structural Mechanics and Materials Laboratory, Department of Mechanical Engineering, Faculty of Technology, University of Chahid Mostefa Ben Boulaïd - Batna 2, Batna 05000, Algeria

Corresponding Author Email: ibrahim.beroual@ummto.dz

https://doi.org/10.18280/rcma.360209

Received: 10 January 2026
Revised: 10 March 2026
Accepted: 19 March 2026
Available online: 30 April 2026

Keywords:
multi-objective optimization, hybrid composite laminates, perforated laminates, torsional loading, genetic algorithm, Tsai-Wu criterion, finite element analysis

ABSTRACT

Stress concentration around holes is a major cause of failure in laminated composite structures, while studies addressing the optimization of their torsional performance remain limited. This study investigates the three-dimensional optimization of hybrid composite laminates based on E-glass, S-glass, and HS-carbon fibers embedded in an epoxy matrix to improve the mechanical response of perforated plates under torsional loading. A multi-objective genetic algorithm (MOGA) implemented in MATLAB and coupled with Pareto-front analysis was used to identify optimal laminate configurations. The design variables included the number of plies (6-12), fiber orientation angle (−90° to 90°), perforated area ratio (5%-25%), hole diameter (10-25 mm), and ply material type, namely HS-carbon/epoxy, E-glass/epoxy, and S-glass/epoxy. A 25% HS-carbon constraint was imposed to enhance stiffness while limiting stress concentrations. The optimization objectives were to maximize the longitudinal modulus (E_x) and shear modulus (G_{xy}) and to minimize the von Mises stress and shear stress, subject to the Tsai-Wu failure criterion. The optimal 11-ply hybrid laminate exhibited substantial improvements compared with a conventional [±45]11 E-glass/epoxy laminate, including a 64% increase in E_x, a 17% reduction in von Mises stress, and a failure index below 0.6 under a torsional moment of 4000 N·mm. The optimization results were further supported by finite element simulations performed in ANSYS, showing consistent trends between the MOGA predictions and numerical analysis. These findings demonstrate the effectiveness of fiber hybridization and multi-objective optimization in improving the torsional behaviour of perforated composite laminates and suggest strong potential for lightweight structural applications requiring enhanced torsional resistance.

1. INTRODUCTION

Composite laminates are ubiquitous structural components in the aerospace, automotive, construction, and marine industries [1-3]. Additionally, the superior mechanical, fatigue, and durability performance of carbon fiber reinforced polymer (CFRP) has enabled its use in many primary structures [4-6]. Assembling different types of materials and components in structures requires holes to facilitate assembly. Thus, drilling holes in composite laminates is common and unavoidable during the design, manufacture, and assembly of structures [7, 8].

Hybrid composites, which combine several types of fibers (such as carbon, glass, and natural or synthetic fibers), allow one to adjust the reinforcement percentages and stacking sequences. This allows overcoming the limitations of homogeneous materials by optimizing specific properties, such as rigidity, impact resistance, and environmental sustainability. For example, work has shown the beneficial effects of an optimal content of 30% by weight and a stacking sequence of palmyra skin and hemp core in unidirectional composite palmyra hemp [9, 10]. Additionally, significant improvements in hardness, impact resistance, and fracture toughness have been achieved through the hybridization of woven E-glass fiber with natural clays and alumina in aerospace applications [11]. For instance, hybridizing carbon and aramid layers with S-glass improves tensile strain, modulus, and flexural properties but slightly reduces tensile strength. Three-point bending tests demonstrate significant improvements in bending properties when S-glass fibers are positioned on the side subjected to compression within the composite thickness [12]. Meanwhile, natural fibers, such as flax and hemp, provide an eco-friendly alternative for lightweight applications [13-15]. However, their behavior under mechanical loading depends heavily on the stress distribution around holes, as the interaction between the layers

affects damage tolerance [16-18].

Perforated laminates are present in many critical structures, such as airplane wings and boat hulls. However, their design must consider the increased stress near holes, which can be 3 to 5 times greater than the nominal stress. According to experimental and numerical studies, the geometry of the holes (e.g., diameter and spacing), their relative position, and the stacking of folds significantly impact failure modes. For instance, nearby holes create synergistic interactions that increase stress concentrations beyond those of an isolated hole [19-24].

Additional shear stresses are introduced by the effect of torsion in perforated laminates, worsening stress concentrations around holes and altering failure modes [3, 25]. Under torsional loading, the anisotropy of composites intensifies interactions between plies, resulting in complex deformations and an increased risk of delamination or interlaminar cracking, especially near perforations [23, 26]. The geometry of the holes and the stacking sequence play a critical role in the distribution of shear stress, requiring specific optimization to minimize torsional damage. Finite element modeling (FEM) captures these complex behaviors by integrating adapted failure criteria to predict torsional resistance and optimize designs [27, 28].

Optimizing hybrid composites requires three-dimensional approaches to adjust key parameters, such as stacking sequence, fiber volume fraction, and ply orientation, to maximize mechanical performance under specific loads [29, 30]. The finite element method (FEM) is a fundamental tool for modeling the mechanical behavior of perforated laminates. It allows for predicting stress distributions and failure modes using advanced criteria, such as Hashin's and Tsai-Wu's [31, 32]. Numerical models validated by experimental techniques, such as acoustic emission and X-ray tomography, provide a thorough understanding of degradation mechanisms in hybrid composites subjected to static [33] and dynamic loading [34]. Recent work also highlights the potential of hybridization to improve damage tolerance; however, the effects of perforations on torsional properties remain understudied [35].

The presence of a hole makes the laminate sensitive to its mechanical properties, which are defined by several factors. These factors include hole dimensions, laminate dimensions, fiber orientations, and ply stacking sequence. Guo et al. [17] studied the mechanical behavior and failure mechanisms of composite laminates with holes under tensile loading using finite element analysis. They modeled carbon-T300/epoxy composite laminates with one, two, or three 10-mm-diameter holes with a stacking sequence of [0°/-30°/30°/-45°/0°/-45°/0°/-45°/90°/0°]. The simulation was performed via ABAQUS with a custom subroutine to capture the progression of failure. The results show that tensile strength is maximal for a single hole and decreases by 20% with three holes. Damage begins near the holes, where stress concentrations are high, and spreads to the edges. The fiber and matrix damage factors increase with hole diameter. The model accurately predicts the initiation and progression of damage. Yang et al. [20] performed a multi-objective optimization of damaged composite laminates repaired with adhesively bonded patches, simultaneously considering static strength and fatigue life. The approach employs a multi-objective genetic algorithm (MOGA / NSGA-II) coupled with FEM simulations to model damage propagation, stress concentrations around the hole/damaged region, and overall repair performance. The optimized variables include patch radius, patch thickness, number of plies, and fiber orientations in both the patch and/or the repaired parent laminate. Fiber orientation sequences commonly used in patches and base plates are typically [0°/±45°/90°] or quasi-isotropic layups. Fibers oriented at 0° enhance axial strength and reduce longitudinal stress concentrations around the hole, while ±45° orientations promote shear energy dissipation and help limit fatigue crack propagation. The transverse (90°) orientations of plies increase transverse stiffness but can increase the risk of local delamination near the hole if not properly balanced. The results demonstrate a significant improvement in both static strength and fatigue life, together with a marked reduction in repair thickness and patch volume. Patches with a radius greater than 14 mm were found to provide a favorable trade-off between high static strength and excellent fatigue resistance. Özaslan et al. [35] studied the stress analysis and strength prediction of composite laminates containing two interactive holes under tensile loading. They analyzed carbon/epoxy laminates with different hole configurations (distances and orientations) by modeling them via the FEM in ABAQUS. The results show that the distance between holes significantly affects stress concentration, resulting in reduced resistance when the holes are close together. An analytical approach based on the method of complex potentials was used to validate the EF results. The main failure modes include matrix cracking and fiber breaking near the holes. Laminates with holes aligned perpendicular to the load exhibit lower resistance than laminates with holes aligned parallel to the load. A resistance prediction model based on the Yamada-Sun criteria was successfully applied. The simulations revealed an increased stress interaction for low inter-hole distance ratios. Wysmulski et al. [36] analyzed the effect of hole diameter on the fracture load and deformation modes of CFRP laminates under axial compression loading. They made CFRP plates with central holes measuring 0 (reference), 2, 4, and 8 mm and tested them using a universal test machine. The tests were carried out with displacement control at 1 mm/min under standard laboratory conditions. Digital image correlation (DIC) analysis captured the local deformations. The results show that the plate without a hole is strongest, with a bearing capacity of 2.6 kN. The plate with an 8 mm hole has a 30% lower bearing capacity. Larger holes lead to localized deformation and asymmetric buckling, which accelerates structural degradation. A nonlinear relationship was observed between hole diameter and breaking load, with a significant drop between 4 and 8 mm. Khan et al. [37] studied the notch sensitivity of carbon/aramid hybrid composite laminates under tensile loading. They manufactured and tested samples with holes of different diameters (with width-to-diameter ratios of 9, 4, 3, and 2) to evaluate mechanical properties. The hybrid laminates included carbon layers and an aramid core made by resin infusion. Tensile tests revealed progressive fracture, including cracking of the matrix, delamination of the folds, and rupture of the fibers near the holes. X-ray images confirmed the absence of initial defects, such as delamination of the folds around the holes. Samples with a w/d ratio of 2 showed increased notch sensitivity, with a significant drop in stress at break. Observed failure modes included localized cracking and fiber buckling at the edges of the holes. These results underscore the significance of the w/d ratio in hybrid composite design. Khechai et al. [38] developed a low-analytical method based on the Greszczuk approach to analyze stresses in non-symmetrical laminated composite plates containing a circular hole under different loadings: axial,

biaxial, and shear. The studied laminates are graphite/epoxy with different fiber orientations and incorporate a finite width correction for plates of actual size. The results show that the stress concentration factor (SCF) reaches a maximum of 4.0 under shear loading when α = 3π/4. Furthermore, stress concentration becomes compressive (with a negative value) for $0 < \alpha < \pi$.

Biaxial loads increase the SCF by 10-20% compared to uniaxial loads. Unlike uniaxial cases, stress distributions become compressive under shear conditions. The analytical method was validated using the FEM, with a deviation of 4.8%. Configurations with fibers at 0° have the highest SCFs near the hole.

This study proposes three-dimensional optimization of the hybridization of E and S-glass and HS-carbon fibers in an epoxy matrix. The focus is on the mechanical behavior of hybrid composite laminates containing holes aligned along the *x*-axis and subjected to torsional moments. Using the FEM and advanced failure criteria, this study evaluates the impact of holes on mechanical performance in terms of their number, diameter, surface area, and center distance. It also identifies the dominant failure mechanisms and proposes an optimized design for high-responsibility structural applications. The results aim to provide recommendations for developing robust, high-performance hybrid composites adapted to advanced industrial requirements.

2. MATERIALS AND METHODS

2.1 Theoretical

2.1.1 Mathematical formulas

The research works [2, 39, 40] demonstrate the mathematical relationship between Hooke's law, which describes the elastic stress–strain relationship, and the linear proportional behavior of stress and strain in elastic materials.

$$\sigma_{ij} = C_{ijkl}\varepsilon_{kl} \tag{1}$$

where, C_{ijkl} is a fourth-order tensor with 81 elastic constants and is the inverted form of Hooke's law for orthotropic materials, as detailed in reference [40].

$$\varepsilon_i = S_{ij}\sigma_j \tag{2}$$

The coefficients S_{ij} are called compliance coefficients, which are the inverse of the stiffness matrix [40].

$$S_{ij} = C_{ij}^{-1} \tag{3}$$

The constitutive Eq. (2) for an orthotropic material can be translated into matrix form [40].

$$\begin{bmatrix}\varepsilon_1\\ \varepsilon_2\\ \varepsilon_3\\ \gamma_{23}\\ \gamma_{13}\\ \gamma_{12}\end{bmatrix} = \begin{bmatrix}S_{11} & S_{12} & S_{13} & 0 & 0 & 0\\ S_{21} & S_{22} & S_{23} & 0 & 0 & 0\\ S_{31} & S_{32} & S_{33} & 0 & 0 & 0\\ 0 & 0 & 0 & S_{44} & 0 & 0\\ 0 & 0 & 0 & 0 & S_{55} & 0\\ 0 & 0 & 0 & 0 & 0 & S_{66}\end{bmatrix}\begin{bmatrix}\sigma_1\\ \sigma_2\\ \sigma_3\\ \tau_{23}\\ \tau_{13}\\ \tau_{12}\end{bmatrix} \tag{4}$$

where, the engineering constants' individual compliance coefficients are [40]:

$$\begin{gathered}S_{11} = {}^{1}/_{E_1},\quad S_{12} = {}^{-\nu_{12}}/_{E_2},\quad S_{13} = {}^{-\nu_{31}}/_{E_3},\\ S_{21} = {}^{-\nu_{12}}/_{E_1}, S_{22} = {}^{1}/_{E_2}, S_{32} = {}^{-\nu_{32}}/_{E_3},\\ S_{31} = {}^{-\nu_{13}}/_{E_1},\quad S_{32} = {}^{-\nu_{23}}/_{E_2},\quad S_{33} = {}^{1}/_{E_3}\\ S_{44} = {}^{1}/_{G_{23}},\ S_{55} = {}^{1}/_{G_{13}}, S_{66} = {}^{1}/_{G_{12}}\\ S_{ij} = S_{ji}\end{gathered} \tag{5}$$

E_1, E_2, and E_3 are the modulus of elasticity in the (1-2-3) coordinate system. *G12, G13,* and *G23* are the shear modulus. The Poisson's ratios are given by υ_{ij} [40].

When the principal material coordinate system is rotated through an angle $\boldsymbol{\theta}$ about the common *z*-axis (3), but does not coincide with the global *x-y-z* coordinate system, the transformed compliance matrix can be defined as [40].

$$[\overline{S}] = [T_2]^{-1}[S][T_1] \tag{6}$$

$$[\overline{S}] = \begin{bmatrix}\overline{S}_{11} & \overline{S}_{12} & \overline{S}_{13} & 0 & 0 & \overline{S}_{16}\\ \overline{S}_{21} & \overline{S}_{22} & \overline{S}_{23} & 0 & 0 & \overline{S}_{26}\\ \overline{S}_{31} & \overline{S}_{32} & \overline{S}_{33} & 0 & 0 & \overline{S}_{36}\\ 0 & 0 & 0 & \overline{S}_{44} & \overline{S}_{45} & 0\\ 0 & 0 & 0 & \overline{S}_{54} & \overline{S}_{55} & 0\\ \overline{S}_{61} & \overline{S}_{62} & \overline{S}_{63} & 0 & 0 & \overline{S}_{66}\end{bmatrix} \tag{7}$$

where, the transformation matrices are T_1 and T_2.

$$T_1 = \begin{bmatrix}c^2 & s^2 & 0 & 0 & 0 & 2cs\\ s^2 & c^2 & 0 & 0 & 0 & -2cs\\ 0 & 0 & 1 & 0 & 0 & 0\\ 0 & 0 & 0 & c & -s & 0\\ 0 & 0 & 0 & s & c & 0\\ -cs & cs & 0 & 0 & 0 & c^2 - s^2\end{bmatrix} \tag{7}$$

$$T_2 = \begin{bmatrix}c^2 & s^2 & 0 & 0 & 0 & cs\\ s^2 & c^2 & 0 & 0 & 0 & -cs\\ 0 & 0 & 1 & 0 & 0 & 0\\ 0 & 0 & 0 & c & -s & 0\\ 0 & 0 & 0 & s & c & 0\\ -2cs & 2cs & 0 & 0 & 0 & c^2 - s^2\end{bmatrix} \tag{9}$$

where, *S* is the compliance matrix of the lamina, $c = cos(\theta)$ and $s = sin(\theta)$. The three-dimensional version of the composite's compliance matrix is substituted into the Classical Laminated Theory (CLT) equations [3].

The fundamental equation for the load-deformation relationship of laminate analysis is presented in Eq. (10) as follows [41]:

$$\begin{Bmatrix}N\\ M\end{Bmatrix} = \begin{bmatrix}A & B\\ B & D\end{bmatrix}\begin{Bmatrix}\varepsilon^0\\ k\end{Bmatrix} \tag{10}$$

{N}, {M}, {ε^0}, and {k} represent the vectors of resultant forces, moments, midplane strains, and curvatures, respectively. The matrices [A], [B], and [D] correspond to extensional stiffness, coupling stiffness, and bending stiffness, respectively. For symmetrical laminates, the coupling matrix [B], which connects extension and bending, is zero. The load-deformation relation in classical lamination theory (CLT) is presented in Eq. (10), according to references [42, 43]. Versions of the matrices [A], [B], and [D] can be written as follows:

$$A_{ij} = \sum_{k=1}^{n} \left[\overline{Q}\right]_k (h_k - h_{k-1}) \quad (11)$$

$$B_{ij} = \frac{1}{2}\sum_{k=1}^{n} \left[\overline{Q}\right]_k (h_k^2 - h_{k-1}^2) \quad (12)$$

$$D_{ij} = \frac{1}{3}\sum_{k=1}^{n} \left[\overline{Q}\right]_k (h_k^3 - h_{k-1}^3) \quad (13)$$

$$h = \sum_{n=1}^{k} t_k \quad (14)$$

$$\left[\overline{Q}\right] = \left[\overline{S}\right]^{-1} \quad (15)$$

where, n is the total number of layers, t_k is the thickness of each layer, and $\left[\overline{Q}\right]_k$ is the transformed reduced stiffness matrix [42]. The plane stress constitutive equation allows for calculating stresses at any z-position within the k[th] layer [40].

$$\{\sigma\}_x = \left[\overline{Q}\right]_k \{\varepsilon\}_x \quad (16)$$

Converting stresses from principal coordinates (x and y) to local coordinates is necessary for calculating von Mises stresses and the Tsai-Wu failure criterion [44]:

$$\{\sigma\}_{12} = [T_2]\{\sigma\}_x \quad (17)$$

Eq. (18) explains the conversion of strains from principal coordinates (x and y) to local coordinates.

$$\{\varepsilon\}_{12} = [T_1]\{\varepsilon\}_x \quad (18)$$

2.1.2 Longitudinal Young's modulus (E_x)

To calculate the effective Young's modulus E_x of a laminate, we must solve the laminate Eq. (10) by reversing it [41].

$$\begin{Bmatrix} \varepsilon^0 \\ k \end{Bmatrix} = \begin{bmatrix} A & B \\ B & D \end{bmatrix}^{-1} \begin{Bmatrix} N \\ M \end{Bmatrix} \quad (19)$$

Since this inversion can be complex, it is simpler to invert the three tensors A, B, and D from Eq. (19) one by one. This allows us to rewrite Eq. (19) as follows [41]:

$$\begin{Bmatrix} \varepsilon^0 \\ k \end{Bmatrix} = \begin{bmatrix} a & b \\ b^T & d \end{bmatrix}^{-1} \begin{Bmatrix} N \\ M \end{Bmatrix} \quad (20)$$

with

$$\begin{aligned} a &= (A - BD^{-1}B)^{-1} \\ d &= (D - BA^{-1}B)^{-1} \\ b &= -aBD^{-1} = -(A - BD^{-1}B)^{-1}BD^{-1} \end{aligned} \quad (21)$$

The following can be defined to determine the laminate's properties [41]:

$$a^* = ha \quad (22)$$

Thus, the effective Young's modulus of the laminate in the x direction is [41]:

$$E_x = {}^1/_{a_{11}^*} \quad (23)$$

2.1.3 Shear modulus (G_{xy})

The in-plane shear modulus G_{xy} of the laminate can be determined from the A_{66} term of the extensional stiffness matrix [45]:

$$G_{xy} = {}^{A_{66}}/_{h} \quad (24)$$

where, h is the total thickness of the laminate and A_{66} is calculated as:

$$A_{66} = \sum_{k=1}^{n} \left[\overline{Q}_{66}\right]_k (h_k - h_{k-1}) \quad (25)$$

where, $\left[\overline{Q}_{66}\right]_k$ is the transformed shear stiffness of the k^{th} ply.

This study uses a genetic algorithm to optimize composite laminates based on CLT. The effective modulus of elasticity (E_x and G_{xy}) obtained for each optimized configuration can be compared to the modulus calculated by FEM.

2.1.4 Shear stress and stress concentration factor

For this study, we focused on calculating two types of stress: shear stress and von Mises stress. The equation below defines the relationship for determining the shear stress near the holes in a composite laminate [46]:

$$\tau_{xy,max\,,\text{with holes}} = K_{xy} \times \tau_{xy,max\,,No\ hole} \quad (26)$$

The shear stress $\tau_{xy,max\,,No\ hole}$ is calculated using Eq. (16), where K_{xy} is the shear stress concentration factor for the laminate, and is defined as follows [47]:

$$K_{xy} = K_t^{\infty}\,(1 + \frac{d}{w}) \quad (27)$$

where, K_t^{∞} is the stress concentration factor for an infinite laminated plate containing a circular hole [48].

$$K_t^{\infty} = 1 + \sqrt{{}^2/_{A_{11}}\left\{\sqrt{A_{11}A_{22}} - A_{12} + \frac{A_{11}A_{22} - A_{12}^2}{2A_{66}}\right\}} \quad (28)$$

2.1.5 The von Mises stress

The von Mises stress is determined by the following formula [49]:

$$\sigma_{VonMises} = \sqrt{{}^1/_2\left((\sigma_x - \sigma_y)^2 + (\sigma_y - \sigma_z)^2 + (\sigma_z - \sigma_x)^2\right) + 3\left(\tau_{xy}^2 + \tau_{yz}^2 + \tau_{xz}^2\right)} \quad (29)$$

where, σ_x, σ_y and σ_z show the normal stresses and τ_{xy}, τ_{yz} and τ_{xz} are the shear stresses in the respective directions.

2.1.6 Tsai-Wu failure criterion

This study used the Tsai-Wu failure criterion to evaluate the progressive degradation of each layer of a hybrid composite laminate. The failure index (FI) for each composite layer was calculated using Eq. (30) [43, 50].

$$\begin{aligned} FI = {} & F_1\sigma_1 + F_2\sigma_{21} + F_3\sigma_3 + F_{11}\sigma_1^2 + F_{22}\sigma_2^2 + \\ & F_{33}\sigma_3^2 + F_{44}\sigma_4^2 + F_{55}\sigma_5^2 + F_{66}\sigma_6^2 + 2F_{12}\sigma_1\sigma_2 + \\ & 2F_{13}\sigma_1\sigma_3 + 2F_{23}\sigma_2\sigma_3 \end{aligned} \quad (30)$$

$$F_1 = {}^1/_{Xt} + {}^1/_{Xc}\,;\ F_2 = {}^1/_{Yt} + {}^1/_{Yc} \quad (31)$$

$$F_3 = {}^{1}/_{Zt} + {}^{1}/_{Zc};\ F_{11} = {}^{-1}/_{Xt \times Xc}$$
$$F_{22} = {}^{-1}/_{Yt \times Yc};\ F_{33} = {}^{-1}/_{Zt \times Zc}$$
$$F_{44} = {}^{1}/_{S_{23}^2};\ F_{55} = {}^{1}/_{S_{13}^2}$$
$$F_{66} = {}^{1}/_{S_{12}^2};\ F_{12} = -\frac{1}{2}\sqrt{F_{11} \times F_{22}};$$
$$F_{23} = -\frac{1}{2}\sqrt{F_{22} \times F_{33}};\ F_{13} = -\frac{1}{2}\sqrt{F_{11} \times F_{33}}$$

In Eq. (31), X, Y, and Z represent the material strengths in the X, Y, and Z directions, respectively. The subscripts t and c denote tensile and compressive strengths, respectively. S denotes the shear strength of the composite laminate. Tensile, compressive, and shear strength values for SG-EP, EG-EP, and CF-EP composites are widely available in the literature, as indicated in references [51-53]. For this study, we used the values in the ANSYS Workbench 16.2 library, as shown in Table 1. The characteristics of the materials used also originate from this library. Negative values indicate compressive strength.

2.2 Problem statement

This study presents 3D numerical analyses of a hybrid composite laminate containing holes aligned along the *x*-axis. The laminate is composed of E-glass/epoxy (EG-EP), S-glass/epoxy (SG-EP), and HS-carbon/epoxy (CF-EP) composite layers. The analyses were performed using ANSYS Workbench with the Anisotropic Composite Preprocessor (ACP) module. The objective of this study is to optimize the laminate to maximize the effective elastic moduli, specifically the longitudinal Young's modulus E_x and the shear modulus G_{xy}, while minimizing the von Mises stress and the shear stress near the holes and respecting the Tsai–Wu failure criterion (≤0.6). The optimization was carried out using an MOGA implemented in MATLAB. A torsional moment was applied to two opposite sides of the hybrid laminated composite plate around the *x*-axis.

The hybrid composite laminate consisted of six to twelve layers, with a total thickness ranging from two to four millimeters. The thickness of each layer was adjusted to meet this constraint. The percent perforated area ranged from 5% to 25%, and the hole diameters ranged from 10 mm to 25 mm. Fiber orientations varied between -90° and 90°. A design constraint required that 25% of the laminate consist of HS-carbon/epoxy (CF-EP) and that all three materials (CF-EP, EG-EP, and SG-EP) be present. The Tsai-Wu failure index was FI ≤ 0.6, and the center distance between the holes was 45 mm. The materials used were EG-EP, SG-EP, and CF-EP. The mechanical properties of the composites are detailed in Table 1.

Table 1. Material properties of reinforced epoxy laminates

Properties [54]	E-Glass/Epoxy	S-Glass/Epoxy	HS-Carbon/Epoxy
Young's Modulus in X-direction (MPa)	40000	50000	121000
Young's Modulus in Y-direction (MPa)	10000	8000	8600
Young's Modulus in Z-direction (MPa)	10000	8000	8600
Poisson's ratio in XY-plane	0.3	0.3	0.27
Poisson's ratio in YZ-plane	0.3	0.3	0.27
Poisson's ratio in XZ-plane	0.4	0.4	0.4
Shear Modulus in XY-plane (MPa)	5000	5000	4700
Shear Modulus in YZ-plane (MPa)	5000	5000	4700
Shear Modulus in XZ-plane (MPa)	3846	3846	3100
Orthotropic Stress Limits			
Tensile strength in X-direction (MPa)	1100	1700	2231
Tensile strength in Y-direction (MPa)	35	35	29
Tensile strength in Z-direction (MPa)	35	35	29
Compressive strength in X-direction (MPa)	-675	-1000	-1082
Compressive strength in Y-direction (MPa)	-120	-120	-100
Compressive strength in Z-direction (MPa)	-120	-120	-100
Shear strength in XY-plane (MPa)	80	80	60
Shear strength in YZ-plane (MPa)	46.15	46.15	32
Shear strength in XZ-plane (MPa)	80	80	60

2.3 Multi-objective genetic algorithm

2.3.1 Genetic algorithm

MOGA is a computer method that solves problems with multiple goals [55]. Instead of finding one perfect solution, MOGA looks for a set of good solutions, known as the Pareto front (see Section 2.3.2). MOGA is useful in engineering and design for tasks such as optimizing structures, managing resources, and modeling complex systems. It helps decision-makers select the optimal solution for their needs. A multi-criteria optimization problem can be described as follows [56]:

Maximize/minimize

$$f_i(x)_i,\ i = 1, \ldots, N \tag{32}$$

Subject to constraints

$$g_j(x) = 0, \quad j = 1, \ldots, M \tag{33}$$

$$h_k(x) \leq 0\ k = 1, \ldots, W \tag{34}$$

where, f_i, g_j and h_k represent the objective functions, equality constraints, and inequality constraints, respectively. N denotes the number of objective functions, and x is an n-dimensional vector.

A genetic algorithm (GA) is a computer method that mimics natural selection and genetics to find solutions. The main components are genes and chromosomes. A chromosome is a sequence of genes. When solving a real-world problem, the genes represent the aspects to be improved upon, while the chromosomes represent possible solutions. GAs search for the best solution by testing many chromosomes. GAs have two advantages: they can test multiple solutions at once, and they

can temporarily accept suboptimal solutions, which prevents them from getting stuck on an average solution [57].

GAs are great for complex problems because they can easily convert variables into genetic sequences that form chromosomes. They explore different paths by maintaining a group of potential solutions. Through operations like crossover and mutation, GAs offer alternative solutions, even if the best solution isn't perfect for reasons not previously considered. This makes GAs useful for designing and optimizing composite structures with layers of materials that have complex properties [43, 58].

A genetic algorithm for multiple goals is called MOGA. MOGA is an improved version of NSGA-II, an algorithm that uses elitism to select optimal solutions. Here's how it works: First, a random group of solutions is created. Then, each solution is evaluated, the best solution is selected, and the solutions are mixed (crossover) and changed (mutation). Elitism helps ensure that the best solutions are used to create new ones. If the results aren't good enough, the process starts over. Ultimately, it provides a set of good solutions known as the Pareto front [59-61].

2.3.2 Pareto approach

Named after Vilfredo Pareto, the Pareto methodology identifies optimal solutions for multi-objective optimization by highlighting a Pareto front: a set of non-dominated solutions where improving one objective compromises another. This approach is useful in science and engineering for balancing conflicting objectives, such as cost/performance or efficiency/sustainability. Visualizations of the Pareto front, as illustrated in Deb's work [55], make it easier to understand the trade-offs involved in complex decision-making [62].

2.3.3 Mathematical formulation of the optimization problem

Objective function:

- Maximize the effective elastic modulus (stiffness).
- Minimize von Mises stress.
- Minimize shear stress.

Design's variables:

- Ply angles: $(-90° \leq \theta \leq 90°)$.
- Ply materials: HS-Carbon/Epoxy (CF-EP), E-Glass/Epoxy (EG-EP), S-Glass/Epoxy (SG-EP).
- Number of plies: Between 6 and 12.
- Thickness ranging from 2 to 4 mm.
- Number of holes.
- The percent perforated area (between 5% and 25%).
- Hole diameters (between 10 mm and 25 mm).

Constraints:

- Tsai-Wu failure index: $FI \leq 0.6$.
- 25% of the plies must be HS-Carbon/Epoxy (CF-EP).
- All three materials (CF-EP, EG-EP and SG-EP) must be present in the laminate.
- Center distance between the holes is 45 mm.

The geometric properties of the composite plate have been defined, including a length of 150 mm and a width of 50 mm. Three torsional tests with moments of 1000 N·mm, 2000 N·mm, and 4000 N·mm were performed on two opposite surfaces of the plate in the *yz*-plane around the *x*-axis.

The first step was configuring the parameters of the MOGA algorithm. An initial population of 100 individuals with a maximum of 100 generations was defined. A larger configuration (200 individuals and 200 generations) was subsequently evaluated, revealing a performance deviation ranging from 1.5% to 2%. Given this moderate discrepancy, the reduced parameters (100 individuals and 100 generations) were retained to limit computational time, which remains particularly high due to the large number of design variables being optimized simultaneously. Increasing the population size or the number of generations would have resulted in prohibitively long computation times without proportional improvement in the quality of the Pareto front. A Pareto fraction was set to retain optimal solutions that demonstrate trade-offs between objectives. To promote exploration of new solutions, a crossover rate of 95% was chosen, and an adaptive mutation function was used to maintain solution diversity. The program displays progress at each iteration, showing the best objective values.

The optimization produced a Pareto front that highlighted the trade-offs between the effective elastic moduli (E_x and G_{xy}) and the maximum von Mises stress and shear stress. An optimal solution was extracted that describes the laminate configuration, including the number of plies, laminate thickness, fiber orientation angles for each ply, number of holes, percent perforated area, hole diameters, stress concentration in each hole, and materials. For this solution, stresses (von Mises and shear) under torsion moments, as well as the maximum Tsai-Wu failure index, were calculated and displayed. The results also include the effective elastic moduli (E_x and G_{xy}), the shear stress in each hole, and the maximum von Mises stress of the optimized hybrid laminated composite.

2.4 Finite element analysis

Finite element analysis (FEA) enables the modeling of composite materials with various simulation tools. ANSYS offers several options for modeling composite materials, including different simulation capabilities. ANSYS ACP is a module that simplifies the definition of required thicknesses and stacking sequences for composite laminates. It includes a layer thickness editor, a stacking sequence editor, a layer arrangement modeling tool, and failure criteria analysis for each layer. Part 2 in Figure 1 illustrates the process for finite element simulation of hybrid composite laminates.

This study involved modeling composite layers made of EG-EP, SG-EP, and CF-EP using ANSYS ACP. This tool allowed us to design composite layers by specifying the thickness of the plies and the orientation of the fibers according to the desired specifications. Next, the hybrid composite material was laminated.

In ANSYS ACP, composite material modeling is performed layer by layer. The process begins in the ACP (Pre) module with creating a sketch of the geometric shape. Then, the structure is refined using an appropriate mesh. Fiber orientations and the stacking sequence are defined using the "stack up" command. Each layer is specified with a distinct material, such as E-glass/epoxy (EG-EP), S-glass/epoxy (SG-EP), or HS-carbon/epoxy (CF-EP). Their mechanical properties, including elastic modulus, Poisson's ratio, and tensile strength, are listed in Table 1. After establishing the geometric model and layer properties, finite element simulations were conducted in ANSYS's "Static Structural" module. In this module, boundary conditions and loads were applied. After execution, the simulation results are displayed, including von Mises stresses, shear stresses, and other results. The Tsai-Wu failure index for the laminate and/or each ply, as well as the effective elastic modulus, is displayed in the ACP (Post) module.

Figure 2 shows the mesh structure and fiber orientations generated by the ACP module. This visualization shows the finite element discretization of the composite model and the precise definition of the ply orientations. These are essential for accurately analyzing the material's anisotropic properties.

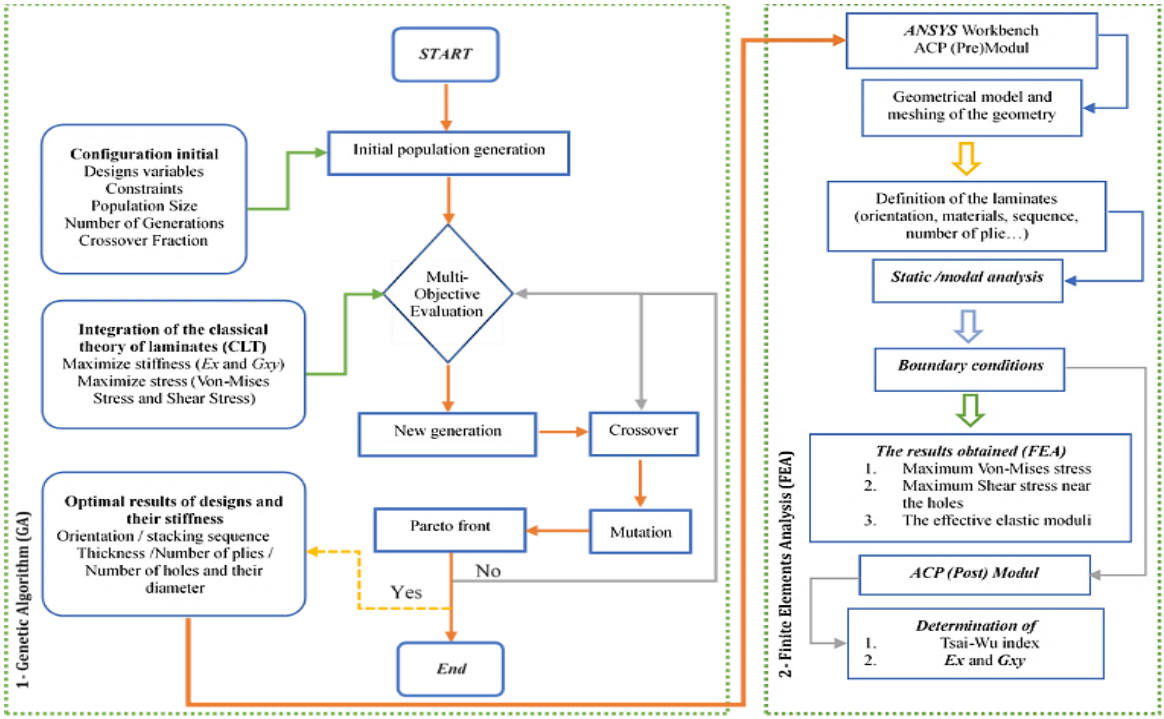

Figure 1. Processing steps of the multi-objective genetic algorithm (MOGA) and finite element analysis (FEA)

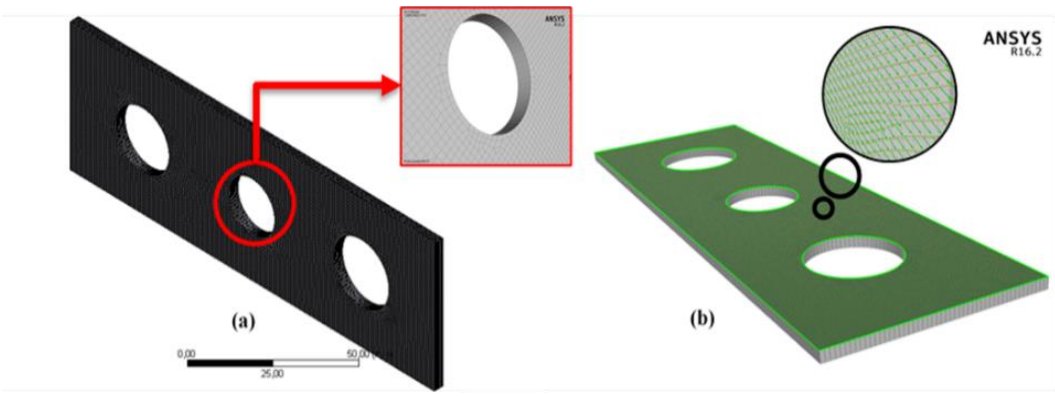

Figure 2. (a) Mesh configuration, (b) fiber orientations in the Anisotropic Composite Preprocessor (ACP) module for the hybrid composite plate

2.5 Mesh independence

Under a torsional moment, a refined mesh with an element size of 1 mm (corresponding to 67470 elements) stabilizes the von Mises stresses at a value of 20.12 MPa, as illustrated in Figure 3. This element size was chosen because it marks the point at which convergence is achieved, thereby minimizing discretization errors and optimizing computational time for maximum efficiency.

To reproduce the torsion test conditions recommended in references [63, 64], two opposing torsional moments were applied to the end faces of the model around the longitudinal *x*-axis. The longitudinal edges were left free to allow warping of the section, as shown in Figure 4.

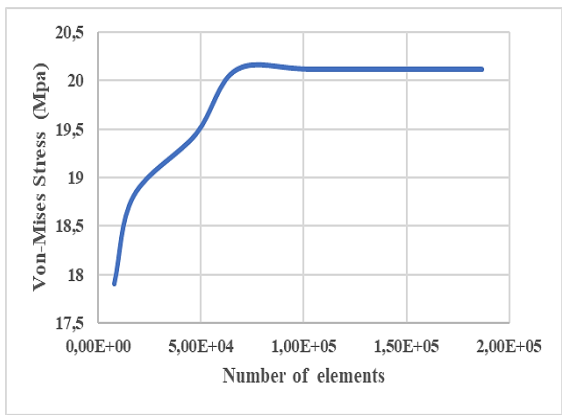

Figure 3. Convergence of von Mises stress as a function of the number of elements

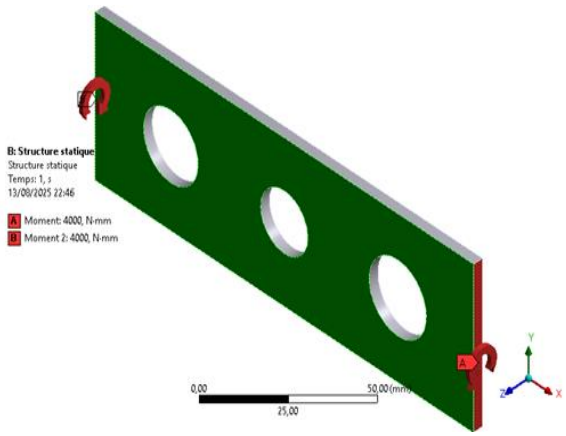

Figure 4. Application of torsional moments on two opposite sides of the laminated composite plate around the *x*-axis

3. RESULTS

3.1 Optimization and finite element analysis results

This section compares the torsion optimization results and properties of hybrid composite laminates obtained through a genetic algorithm implemented in MATLAB with those simulated using the FEM. The comparisons are accompanied by thorough discussions.

3.1.1 Multi-objective genetic algorithm results

The optimization results of hybrid composite laminates under torsional moments, obtained through a genetic algorithm, are presented in Tables 2 and 3. The optimization process used a population of 100 individuals and up to 100 generations to determine the laminate properties. For a torsional moment of 1000 N·mm, the optimization produced a 10-layer hybrid laminate with three holes at the following coordinates and diameters: (-45 mm, 0 mm, 45 mm) and 16.14 mm, 21.74 mm, and 17.9 mm, respectively. This resulted in a perforated area of 11.02%. The laminate's stacking sequence was $[-77_{SG\text{-}EP}/79_{EG\text{-}EP}/77_{CF\text{-}EP}/-81_{SG\text{-}EP}/53_{SG\text{-}EP}/-51_{SG\text{-}EP}/24_{SG\text{-}EP}/0_{CF\text{-}EP}/68_{CF\text{-}EP}/47_{SG\text{-}EP}]$, exhibiting maximum von Mises stress of 22.568 MPa and maximum shear stress of 11.54, 11.72, and 9.021 MPa at the hole coordinates (-45 mm, 0 mm, 45 mm). It also exhibited a longitudinal Young's modulus of 23380 MPa, a shear modulus of 8335 MPa, a Tsai-Wu failure index of 0.188, and a thickness of 3.69 mm.

Running the optimization program with a torsion moment of 2000 N·mm resulted in an 11-layer hybrid laminate with three holes at the following coordinates: (-45 mm, 0 mm, and 45 mm). The respective diameters were 20.7 mm, 21.9 mm, and 15.8 mm. This resulted in a perforated area of 12.12%. The laminate had the following stacking sequence: $[12_{SG\text{-}EP}/6_{CF\text{-}EP}/-24_{SG\text{-}EP}/-46_{CF\text{-}EP}/54_{SG\text{-}EP}/-37_{SG\text{-}EP}/87_{CF\text{-}EP}/-43_{SG\text{-}EP}/-22_{EG\text{-}EP}/15_{EG\text{-}EP}/0_{EG\text{-}EP}]$. It showed a maximum von Mises stress of 37.517 MPa and maximum shear stresses of 21.66 MPa, 17.382 MPa, and 17.182 MPa at the coordinates (-45 mm, 0 mm, and 45 mm), respectively. It also showed a longitudinal Young's modulus of 35978 MPa, a shear modulus of 10037 MPa, and a Tsai-Wu failure index of 0.261, and a laminate thickness of 3.6 mm. A 11-layer hybrid laminate with three holes at the aforementioned coordinates and with diameters of 21.7 mm, 18.73 mm, and 22.7 mm, respectively, resulted in a perforated area of 14% for a torsion moment of 4000 N·mm. The laminate had a stacking sequence $[8_{EG\text{-}EP}/13_{SG\text{-}EP}/-3_{EG\text{-}EP}/26_{SG\text{-}EP}/-2_{SG\text{-}EP}/14_{SG\text{-}EP}/25_{EG\text{-}EP}/-30_{CF\text{-}EP}/-43_{CF\text{-}EP}/-17_{CF\text{-}EP}/-16_{EG\text{-}EP}]$ and was characterized by a maximum von Mises stress of 69.017 MPa. The maximum shear stresses τ_{xy} near the holes were 26.293 MPa, 18.022 MPa, and 27.208 MPa at the coordinates (-45 mm, 0 mm, 45 mm). The laminate also had a longitudinal Young's modulus E_x of 48341 MPa, a shear modulus G_{xy} of 8986 MPa, and a Tsai–Wu failure index of 0.54, and a laminate thickness of 3.55 mm.

Table 2. Presentation of torsional moments optimization results

Torsional Moments	Stacking Sequence	Thickness of Laminate (mm)	Number of Holes	Von Mises Stresses (MPa)	Shear Moduli (MPa)	Young's Moduli (MPa)	Tsai-Wu Index
1000 N·mm	$[-77_{SG\text{-}EP}/79_{EG\text{-}EP}/77_{CF\text{-}EP}/-81_{SG\text{-}EP}/53_{SG\text{-}EP}/-51_{SG\text{-}EP}/24_{SG\text{-}EP}/0_{CF\text{-}EP}/68_{CF\text{-}EP}/47_{SG\text{-}EP}]$	3.69	3	22.568	8335	23380	0.188
2000 N·mm	$[12_{SG\text{-}EP}/6_{CF\text{-}EP}/-24_{SG\text{-}EP}/-46_{CF\text{-}EP}/54_{SG\text{-}EP}/-37_{SG\text{-}EP}/87_{CF\text{-}EP}/-43_{SG\text{-}EP}/-22_{EG\text{-}EP}/15_{EG\text{-}EP}/0_{EG\text{-}EP}]$	3.6	3	37.517	10037	35978	0.261
4000 N·mm	$[8_{EG\text{-}EP}/13_{SG\text{-}EP}/-3_{EG\text{-}EP}/26_{SG\text{-}EP}/-2_{SG\text{-}EP}/14_{SG\text{-}EP}/25_{EG\text{-}EP}/-30_{CF\text{-}EP}/-43_{CF\text{-}EP}/-17_{CF\text{-}EP}/-16_{EG\text{-}EP}]$	3.55	3	69.017	8986	48341	0.549

Table 3. Presentation of shear stresses near the holes and characteristics of holes for optimization results

Torsional Moments	Stacking Sequence	Diameter of Hole 1 (mm) Coordinate (-45 mm)	Diameter of Hole 2 (mm) Coordinate (0 mm)	Diameter of Hole 3 (mm) Coordinate (45 mm)	Shear Stress of Hole 1 (MPa)	Shear Stress of Hole 2 (MPa)	Shear Stress of Hole 3 (MPa)
1000 N·mm	$[-77_{SG\text{-}EP}/79_{EG\text{-}EP}/77_{CF\text{-}EP}/-81_{SG\text{-}EP}/53_{SG\text{-}EP}/-51_{SG\text{-}EP}/24_{SG\text{-}EP}/0_{CF\text{-}EP}/68_{CF\text{-}EP}/47_{SG\text{-}EP}]$	16.14	21.74	17.87	11.54	11.72	9.021

2000 N·mm	[12_{SG-EP}/6_{CF-EP} /-24_{SG-EP}/-46_{CF-EP} /54_{SG-EP} /-37_{SG-EP}/87_{CF-EP} /-43_{SG-EP} /-22_{EG-EP} /15_{EG-EP}/0_{EG-EP}]	20.7	21.9	15.8	21.66	17.382	17.182
4000 N·mm	[8_{EG-EP}/13_{SG-EP} /-3_{EG-EP}/26_{SG-EP}/-2_{SG-EP} /14_{SG-EP}/25_{EG-EP} /-30_{CF-EP} /-43_{CF-EP} /-17_{CF-EP}/-16_{EG-EP}]	21.7	18.73	22.7	26.293	18.022	27.208

Tables 2 and 3 illustrate a Multiphysics optimization approach:

• For each torsional load level, a specific stacking sequence is selected.

• The laminate thickness decreases slightly despite the increasing load thanks to ply optimization.

• The presence of holes induces local stress concentrations, which are accounted for in the design.

The employed method appears to combine mechanical analysis, numerical optimization, and validation via the Tsai-Wu index, which is required to be ≤ 1 for acceptance and strictly < 0.6 in the present optimized designs. The results are presented systematically, facilitating interpretation and reproducibility in a research or engineering context.

Across the optimal stacking sequences, several design principles emerge to balance torsional stiffness, stress mitigation around holes, and overall structural integrity. Carbon fiber plies (CF-EP) are predominantly oriented near 0° (e.g., 0° in the 1000 and 2000 N·mm designs) to maximize Young's longitudinal modulus E_x, which increases progressively with load (from 23380 MPa to 48341 MPa), while also incorporating angles near ±45° (e.g., -46° at 2000 N·mm, -43° and -30° at 4000 N·mm) to enhance shear modulus *Gxy* and handle torsional shear flows effectively. S-glass plies (SG-EP), known for higher strength and impact resistance, are frequently placed at intermediate angles around ±45°-55° (e.g., 53°, -51°, and 47° at 1000 N·mm; 54°, -37°, and -43° at 2000 N·mm) and appear clustered in positions that likely mitigate stress concentrations near the holes, as evidenced by the controlled shear stresses (e.g., dropping to 9-11 MPa at 1000 N·mm despite holes). E-glass plies (EG-EP), offering cost-effective stiffness, are used sparingly at varied angles (e.g., near 0°-15° in higher loads) to fine-tune the laminate's transverse properties without excessive weight. This hybrid material strategy shifts from high-angle dominance in low loads (for transverse support) to low-angle emphasis in high loads (for axial reinforcement), enabling thickness reduction while keeping Tsai-Wu indices below 0.6 and von Mises stresses manageable, thus turning empirical optimization into robust, load-adaptive composite designs.

3.1.2 Finite element analysis results

The simulation aimed at calculating the equivalent von Mises stress, the shear stress near the holes, the effective elastic moduli (E_x and G_{xy}) and the Tsai-Wu failure index for the configurations of hybrid composite laminates containing holes obtained via a MOGA. The analyses were performed using the ANSYS Workbench 16.2 finite element solver. This analysis provided essential information on the mechanical behavior of the hybrid composite laminates containing the holes. Figures 5-7 illustrate the distribution of von Mises stresses, shear stress, and Tsai-Wu failure index for hybrid composite laminates under torsional moments, as obtained from the simulation with a mesh size of 1.0 mm.

Firstly, for torsion moment of 1000 N·mm with the stacking sequence [-77_{SG-EP}/79_{EG-EP}/77_{CF-EP}/-81_{SG-EP}/53_{SG-EP}/-51_{SG-EP}/24_{SG-EP}/0_{CF-EP} /68_{CF-EP}/47_{SG-EP}], exhibiting a maximum von Mises stress of 20.12 MPa, maximum shear stresses τ_{xy} near the holes of 10.106 MPa, 9.438 MPa, and 9.937 MPa, respectively, at coordinates (-45 mm, 0 mm, 45 mm), a longitudinal Young's modulus E_x of 24468.3 MPa, a shear modulus G_{xy} of 8937.56 MPa and Tsai-Wu failure index of 0.147.

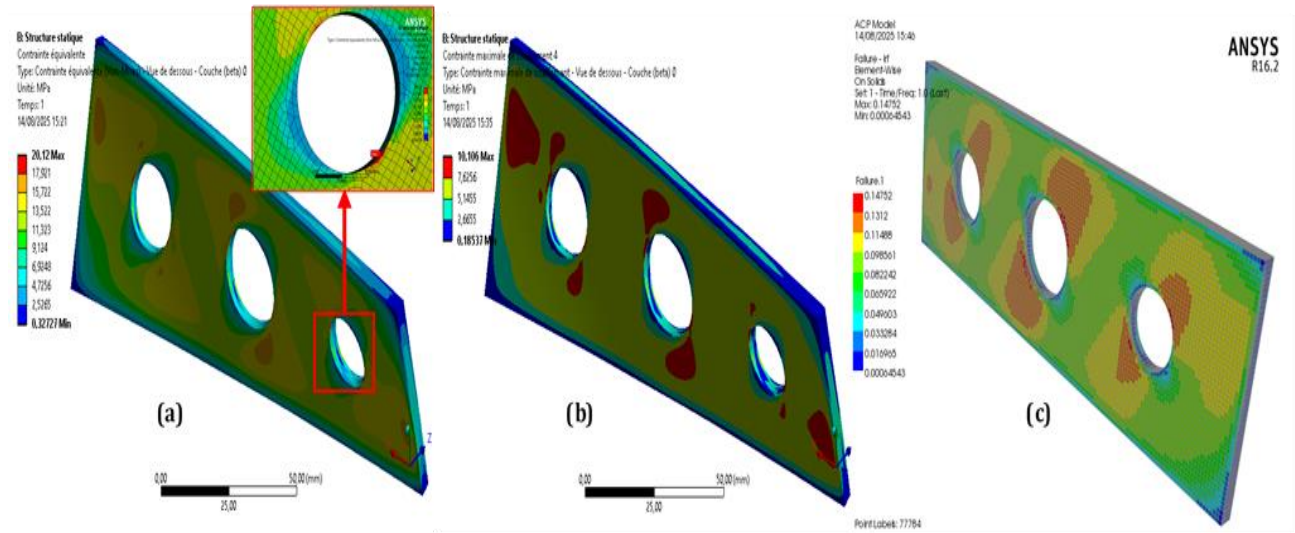

Figure 5. The Von Mises stress, Shear stress and Tsai-Wu failure index of the hybrid composite laminate [-77_{SG-EP}/79_{EG-EP}/77_{CF-EP}/-81_{SG-EP}/53_{SG-EP}/-51_{SG-EP}/24_{SG-EP} /0_{CF-EP}/68_{CF-EP}/47_{SG-EP}] subjected to a torsional moment of 1000 N·mm. (a) Von Mises stress, (b) Shear stress, (c) Tsai-Wu failure index

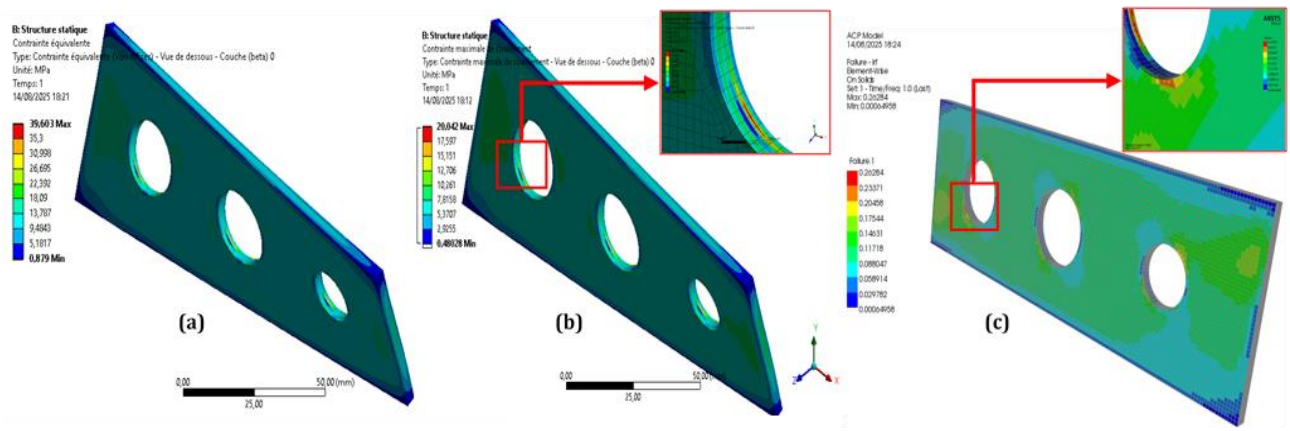

Figure 6. The Von Mises stress, Shear stress and Tsai-Wu failure index of the hybrid composite laminate [$12_{SG\text{-}EP}/6_{CF\text{-}EP}/\text{-}24_{SG\text{-}EP}/\text{-}46_{CF\text{-}EP}/54_{SG\text{-}EP}/\text{-}37_{SG\text{-}EP}/87_{CF\text{-}EP}/\text{-}43_{SG\text{-}EP}/\text{-}22_{EG\text{-}EP}/15_{EG\text{-}EP}/0_{EG\text{-}EP}$] subjected to torsional moment of 2000 N·mm. (a) Von Mises stress, (b) Shear stress, (c) Tsai-Wu failure index

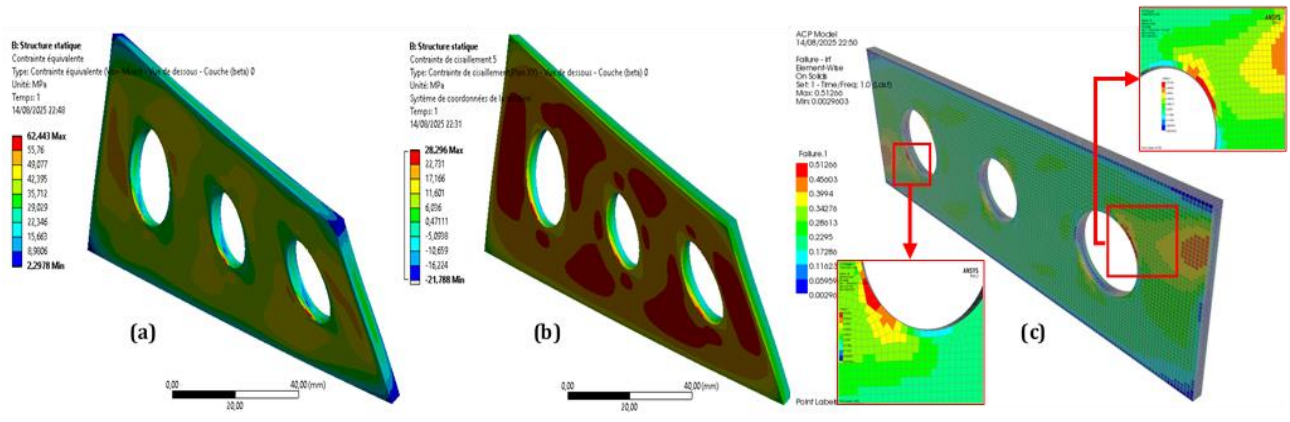

Figure 7. The Von Mises stress, Shear stress and Tsai-Wu failure index of the hybrid composite laminate [$8_{EG\text{-}EP}/13_{SG\text{-}EP}/\text{-}3_{EG\text{-}EP}/26_{SG\text{-}EP}/\text{-}2_{SG\text{-}EP}/14_{SG\text{-}EP}/25_{EG\text{-}EP}/\text{-}30_{CF\text{-}EP}/\text{-}43_{CF\text{-}EP}/\text{-}17_{CF\text{-}EP}/\text{-}16_{EG\text{-}EP}$] subjected to torsional moment of 4000 N·mm. (a) Von Mises stress, (b) Shear stress, (c) Tsai-Wu failure index

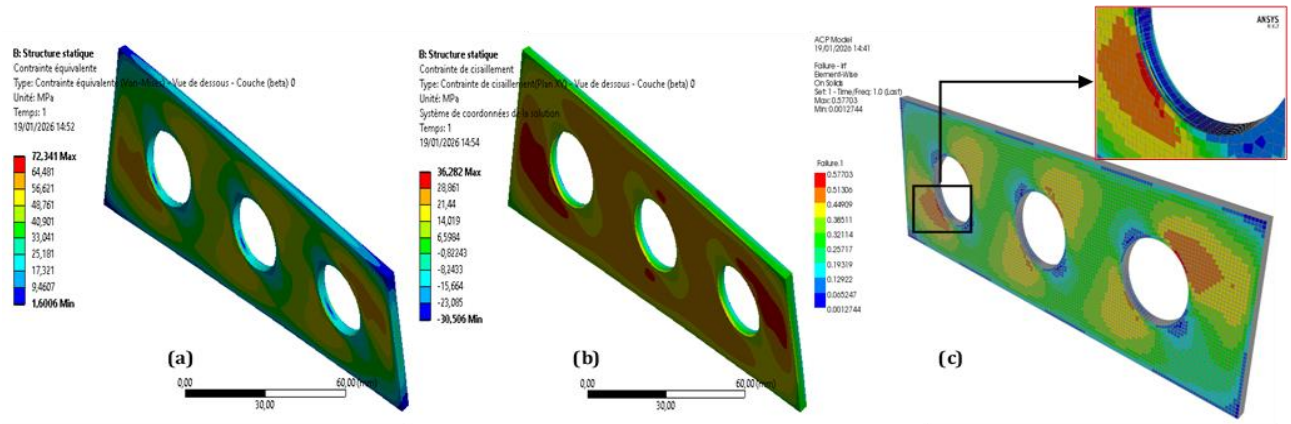

Figure 8. The Von Mises stress, Shear stress and Tsai-Wu failure index of conventional $[\pm 45]_{11}$ E-glass/epoxy laminate subjected to torsional moment of 4000 N·mm. (a) Von Mises stress, (b) Shear stress, (c) Tsai-Wu failure index

Next, for torsion moment of 2000 N·mm with the stacking sequence [$12_{SG\text{-}EP}/6_{CF\text{-}EP}/\text{-}24_{SG\text{-}EP}/\text{-}46_{CF\text{-}EP}/54_{SG\text{-}EP}/\text{-}37_{SG\text{-}EP}/87_{CF\text{-}EP}/\text{-}43_{SG\text{-}EP}/\text{-}22_{EG\text{-}EP}/15_{EG\text{-}EP}/0_{EG\text{-}EP}$], characterized by a maximum von Mises stress of 39.603 MPa, maximum shear stresses τ_{xy} near the holes of 20.042 MPa, 18.251 MPa, and 18.769 MPa, respectively, at coordinates (-45 mm, 0 mm, 45 mm), a longitudinal Young's modulus E_x of 36728.8 MPa, a shear modulus G_{xy} of 10200.5 MPa and Tsai-Wu failure index of 0.262.

Finally, for torsion moment of 4000 N·mm with the stacking sequence [$8_{EG\text{-}EP}/13_{SG\text{-}EP}/\text{-}3_{EG\text{-}EP}/26_{SG\text{-}EP}/\text{-}2_{SG\text{-}EP}/14_{SG\text{-}EP}/25_{EG\text{-}EP}/\text{-}30_{CF\text{-}EP}/\text{-}43_{CF\text{-}EP}/\text{-}17_{CF\text{-}EP}/\text{-}16_{EG\text{-}EP}$], presented a maximum von Mises stress of 62.443 MPa, maximum shear stresses τ_{xy} near the holes of 25.117 MPa, 24.142 MPa, and 25.28 MPa, respectively, at coordinates (-45 mm, 0 mm, 45 mm), a longitudinal Young's modulus E_x of 44063.3 MPa, a shear modulus G_{xy} of 10381.7 MPa and Tsai-Wu failure index of 0.512.

4. DISCUSSION

The presence of circular holes in composite laminates, as defined by their geometric parameters (number, diameter, and spacing), significantly alters the mechanical behavior and properties of these materials. This alteration primarily results from the stress concentration phenomenon that occurs near the holes, as demonstrated by Guo et al. [17] and Özaslan et al. [35]. The ultimate strength of such plates is influenced by numerous parameters that have been extensively studied, including loading type, stacking sequence, number of plies, and hole diameter. Configurations dominated by 0°-oriented plies are distinguished by the highest stress concentration factors near the holes [38]. Furthermore, increasing hole size leads to a significant reduction in failure load, as shown by experimental compression tests. Tensile test results also confirm that the structural strength of composite laminates decreases as the number of holes increases [65]. These observations are consistent with the challenges identified in the present study.

According to the results of the MOGA optimization, a clear trend emerges in the stacking sequences optimized for increasing torsional moments (from 1000 N·mm to 4000 N·mm). The number of plies in SG-EP (S-glass fiber impregnated with epoxy resin) decreases progressively (from six to four plies), while the number of plies in EG-EP (E-glass fiber) increases (from one to four plies). The number of plies in CF-EP (carbon fiber) remains fixed at three. This is in response to the constraint imposed to prevent the carbon fiber content from exceeding 25% of the total number of plies. This redistribution is due to the superior properties of S-glass fiber, particularly its significantly higher modulus of elasticity. This gives S-glass fiber a better capacity to withstand high local shear and tensile stresses around holes under moderate loads. However, as the torsional moment increases, E-glass fiber is favored in greater numbers to ensure more homogeneous load distribution and avoid excessive overall stiffness, which could lead to localized failure.

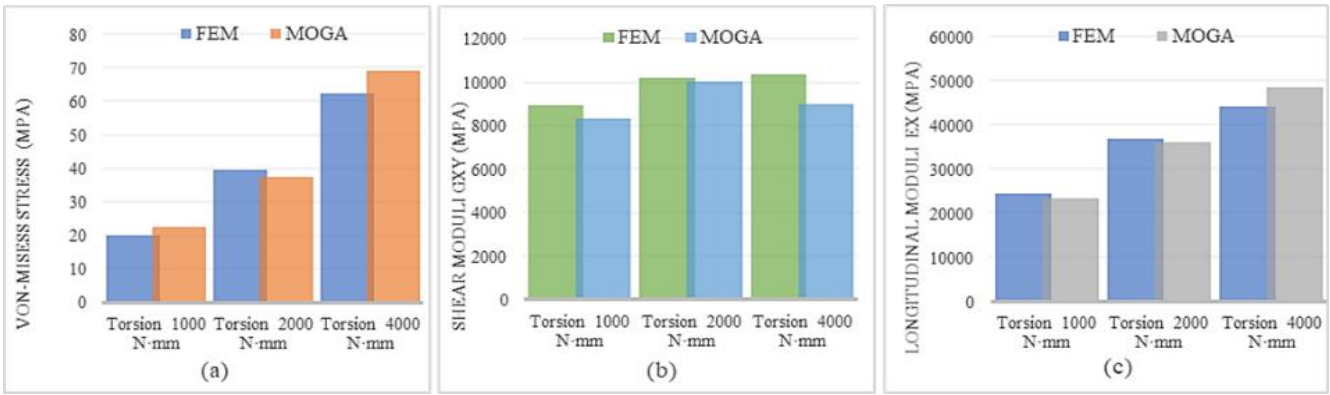

Figure 9. Comparison between FEM and MOGA results for torsional moments. (a) Von Mises stress, (b) Shear moduli G_{xy}, (c) Longitudinal Young's Moduli E_x

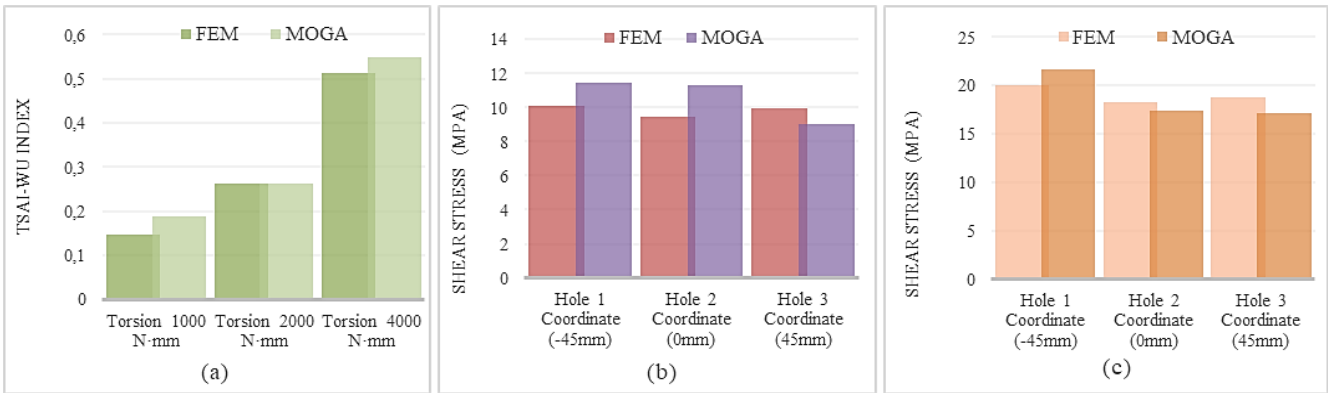

Figure 10. Comparison between FEM and MOGA results for torsional moments. (a) Tsai-Wu index, (b) Shear stress near the holes for torsion moment of 1000 N·mm, (c) Shear stress near the holes for torsion moment of 2000 N·mm

The sequences optimized by MOGA significantly outperform the pure EG-EP [±45] laminate, which is considered the optimal baseline configuration for pure shear in torsion. Finite element simulations were performed on a pure EG-EP [±45] laminate with fair diameter holes under a torsional loading of 4000 N·mm. The laminate had the same dimensions and number of plies as the optimized sequence for this load level. The pure EG-EP [±45] laminate exhibits inferior performance, including a limited increase in longitudinal stiffness and higher von Mises and shear stress peaks, as well as a larger Tsai-Wu failure index. Figure 8 illustrates the finite element simulation results obtained for the conventional $[\pm 45]_{11}$ laminate. The optimized sequences strategically place very high-modulus CF-EP plies at intermediate or high angles (for example, close to ±77° to ±81° in some cases, or ±43° to ±87° in others), while distributing the more compliant SG-EP and EG-EP plies (offering better shear compliance and higher strain-to-failure) in critical zones to dampen stress gradients. The optimized ply angles (±70° to ±81° at lower torsion moments, shifting closer to ±45° at

higher moments) position the fibers in a configuration that minimizes direct loading in the regions of highest shear flow perturbation around the hole. This significantly reduces the local shear stress concentration factor in these critical zones. At the same time, these angles remain sufficiently distant from 0°/90° to maintain high in-plane shear stiffness, thereby enabling efficient uptake and more diffuse redistribution of the torsional shear flow across a broader area of the laminate. The alternation between high-modulus CF-EP plies (at intermediate/high angles) and more compliant SG-EP/EG-EP plies further smooths local shear strain gradients and mitigates sharp shear stress peaks. This non-classical angular dispersion accounts for the observed improvements over the pure [±45] EG-EP baseline: 64% increase in the longitudinal Young's modulus E_x, 17% reduction in the von Mises equivalent stress, 29% reduction in the maximum shear stress τ_{xy}, and 12% decrease in the Tsai-Wu failure index. This hybridization of materials, combined with an unconventional angular dispersion, generates several highly favorable synergistic effects under torsional loading. Indeed, fiber angles near ±45° to ±80° allow for a particularly efficient uptake of torsional shear stress due to the directional stiffness of the fibers, while avoiding direct alignment with the high-stress tensile zones generated around the holes. This configuration leads to a significant reduction in shear stress τ_{xy} peaks around the holes, promoting a much more uniform distribution of shear flow across the entire width of the laminate. Furthermore, the alternation between plies with very high longitudinal stiffness (CF-EP) and the more compliant plies (SG-EP and EG-EP) creates a progressive stiffness transition around the holes, which substantially reduces the effective stress concentration factor compared to single-material or non-hybrid laminates. The literature on notched hybrid composites often confirms that this type of hybridization delays the onset of local damage by smoothing out stress discontinuities between plies. Finally, the strategic placement of SG-EP plies with high shear strength in the outer layers or within critical thickness zones strongly minimizes matrix-dominated shear failure modes around the holes. The extremely low Tsai-Wu indices systematically achieved (always below 0.6 and validated by finite element analysis) thus demonstrate a particularly balanced and efficient utilization of the directional strengths of the different materials, without excessive stress localization.

The present work, therefore, aims to optimize hybrid composite laminates containing holes and subjected to torsional loading, using the Tsai-Wu failure criterion as the primary constraint to prevent premature laminate failure. Our analyses highlight the significant influence of fiber orientation, material stacking sequence (CF-EP, EG-EP, SG-EP), as well as hole diameter and number, on the mechanical behavior of perforated hybrid laminates under torsional moments. For example, the hybrid laminate with the stacking sequence $[-77_{SG\text{-}EP}/79_{EG\text{-}EP}/77_{CF\text{-}EP}/-81_{SG\text{-}EP}/53_{SG\text{-}EP}/-51_{SG\text{-}EP}/24_{SG\text{-}EP}/0_{CF\text{-}EP}/68_{CF\text{-}EP}/47_{SG\text{-}EP}]$ exhibits distinct behavior under a torsional moment of 1000 N·mm (Figure 5), characterized by high strength, reduced stresses, and a very low Tsai-Wu failure index. This result, obtained via MOGA and compared to finite element results, shows excellent agreement, with percentage errors of 10.85% for the von Mises stress, 6.74% for the shear modulus G_{xy}, 4.45% for the longitudinal Young's modulus E_x, 21.80% for the Tsai-Wu index, and (11.8%, 16.27%, 9.21%) for the maximum shear stresses τ_{xy} around the holes at coordinates (-45 mm, 0 mm, 45 mm), respectively. Detailed comparisons for the entire study are presented in Figures 9 and 10. Similar trends are observed for higher torsional moments (2000 N·mm and 4000 N·mm) shows in Figures 6 and 7, respectively, with the corresponding optimized sequences generally yielding errors below 10 to 15% for key quantities, confirming the robustness of the approach.

The FEM and MOGA methods are useful for studying hybrid composite laminates with holes. These methods provide similar results with minimal error for the Tsai-Wu index: 0.38% error in the torsional moment of 2000 N·mm and 1.60% and 2.04% error in the elastic modulus under the same loading. This proves that they accurately predict stress. Simulations performed using ANSYS Workbench and a genetic algorithm implemented in MATLAB enable robust analysis under various loadings and provide a solid foundation for optimization. These tools help us better understand laminate behavior, particularly as it relates to fiber orientations, stacking sequences, and the presence of holes. The diameter and number of holes significantly affect stress distribution and structural integrity; larger or more numerous holes increase stress concentrations and potentially elevate the risk of failure under torsional loads.

5. CONCLUSION

This study optimized the mechanical behavior of hybrid composite laminates containing holes and subjected to torsional moments. The laminates were made of HS-carbon/epoxy (CF-EP), E-glass/epoxy (EG-EP), and S-glass/epoxy (SG-EP). A MOGA implemented in MATLAB was used for optimization. The results obtained by MOGA are validated by the FEM, which shows good agreement with the optimization results. Despite their impact on mechanical properties, holes in composite laminates are often necessary for functional, structural, or weight-reduction purposes. The optimization process systematically positioned the fibers within the angular range of [−90°, +90°]. Unlike conventional orientations (0°, ±45°, and ±90°), high-strength (HS) carbon fibers are placed in the mid-plane, limited to a maximum of three plies, to effectively resist torsional shear. Concurrently, S-glass fibers, which provide superior stiffness, significantly greater transverse tensile strength, and enhanced interlaminar shear resistance, are preferentially positioned in the laminate's outer plies. This hybrid layup strategy combines the very high longitudinal torsional stiffness and strength of the central HS carbon plies with the enhanced damage tolerance, improved energy dissipation, and better protection against sudden catastrophic failure of the outer S-glass layers.

The following main conclusions were reached:

- Hybridizing the three materials (CF-EP, EG-EP, and SG-EP) and optimizing fiber orientation enhances stiffness and reduces the Tsai-Wu failure index while controlling von Mises and shear stresses.
- The presence of holes alters the local stiffness of the structure and limits its load-carrying capacity due to stress concentration near the holes.
- The number and diameter of the holes have a strong influence on laminate failure.

Among the main limitations of this study is the absence of experimental validation, as well as the neglect of thermal and humidity-related parameters.

In the framework of future work, an experimental investigation on hybrid laminates containing holes sheets is

planned. This campaign will notably include mechanical testing (for example, torsion and cyclic fatigue testing) under controlled hygrothermal conditions.

REFERENCES

[1] Jones, R.M. (2018). Mechanics of Composite Materials. CRC Press. https://doi.org/10.1201/9781498711067

[2] Daniel, I.M., Ishai, O. (1994). Engineering Mechanics of Composite Materials. New York: Oxford University Press.

[3] Kaw, A.K. (2005). Mechanics of Composite Materials. CRC Press. https://doi.org/10.1201/9781420058291

[4] Xian, G., Guo, R., Li, C., Hong, B. (2023). Mechanical properties of carbon/glass fiber reinforced polymer plates with sandwich structure exposed to freezing-thawing environment: Effects of water immersion, bending loading and fiber hybrid mode. Mechanics of Advanced Materials and Structures, 30(4): 814-834. https://doi.org/10.1080/15376494.2021.2024927

[5] Pan, Y., Yan, D. (2021). Study on the durability of GFRP bars and carbon/glass hybrid fiber reinforced polymer (HFRP) bars aged in alkaline solution. Composite Structures, 261: 113285. https://doi.org/10.1016/j.compstruct.2020.113285

[6] Guo, R., Li, C., Xian, G. (2023). Water absorption and long-term thermal and mechanical properties of carbon/glass hybrid rod for bridge cable. Engineering Structures, 274: 115176. https://doi.org/10.1016/j.engstruct.2022.115176

[7] Tai, J.L., Grzejda, R., Sultan, M.T.H., Łukaszewicz, A., Shahar, F.S., Tarasiuk, W., Rychlik, A. (2023). Experimental investigation on the corrosion detectability of A36 low carbon steel by the method of phased array corrosion mapping. Materials, 16(5): 5297. https://doi.org/10.3390/ma16155297

[8] Zheng, K., Hu, H., Cao, D., Zhong, Y., Li, S. (2023). Experimental and numerical studies on the tensile behaviors of thin-ply and thick-ply open-hole laminates. Thin-Walled Structures, 186: 110649. https://doi.org/10.1016/j.tws.2023.110649

[9] Sathishkumar, T.P., Naveen, J., Satheeshkumar, S. (2014). Hybrid fiber reinforced polymer composites–A review. Journal of Reinforced Plastics and Composites, 33(5): 454-471. https://doi.org/10.1177/0731684413516393

[10] Narayana, V.L., Rao, L.B., Devireddy, S.B.R. (2020). Effect of fiber percentage and stacking sequence on mechanical performance of unidirectional hemp and palmyra reinforced hybrid composites. Revue des Composites et des Matériaux Avancés, 30: 153-160. https://doi.org/10.18280/rcma.303-405

[11] Al-Attar, A.F., Jaber, H.A., Hasan, A.M. (2023). Enhancement of mechanical properties in glass-fiber woven reinforced hybrid composites for aerospace applications: An empirical investigation. Revue des Composites et des Matériaux Avancés, 33(6): 347-355. https://doi.org/10.18280/rcma.330601

[12] Alsaadi, M., Erkliğ, A., Alrawi, H. (2017). Effect of S-glass fabric on the mechanical characteristics of a hybrid carbon/aramid fabric reinforced epoxy composites. Materials Research Express, 4(5): 055304. https://doi.org/10.1088/2053-1591/aa6bab

[13] Maiti, S., Islam, M.R., Uddin, M.A., Afroj, S., Eichhorn, S.J., Karim, N. (2022). Sustainable fiber-reinforced composites: A review. Advanced Sustainable Systems, 6(11): 2200258. https://doi.org/10.1002/adsu.202200258

[14] Lin, T.L., Jang, B.Z. (1990). Fracture behavior of hybrid composites containing both short and continuous fibers. Polymer Composites, 11(5): 291-300. https://doi.org/10.1002/pc.750110507

[15] Mohanraj, C.M., Rameshkumar, R., Mariappan, M., Mohankumar, A., et al. (2025). Recent progress in fiber reinforced polymer hybrid composites and its challenges-A comprehensive review. Journal of Natural Fibers, 22(1): 2495911. https://doi.org/10.1080/15440478.2025.2495911

[16] Nunna, S., Chandra, P.R., Shrivastava, S., Jalan, A.K. (2012). A review on mechanical behavior of natural fiber based hybrid composites. Journal of Reinforced Plastics and Composites, 31(11): 759-769. https://doi.org/10.1177/0731684412444325

[17] Guo, Z., Shi, H., Kuai, P., Wei, S., Ma, S. (2022). Finite element analysis of the failure behaviour and mechanism of composite laminates with holes under tension. Journal of Materials Science and Metallurgy, 3: 104.

[18] Nguyen-Hoang, M., Becker, W. (2022). Open holes in composite laminates with finite dimensions: structural assessment by analytical methods. Archive of Applied Mechanics, 92(3): 1101-1125. https://doi.org/10.1007/s00419-021-02095-w

[19] Sihn, S., Kim, R.Y., Kawabe, K., Tsai, S.W. (2007). Experimental studies of thin-ply laminated composites. Composites Science and Technology, 67(6): 996-1008. https://doi.org/10.1016/j.compscitech.2006.06.008

[20] Yang, X., Wu, Z., Zheng, J., Lei, H., Liu, L., Chen, W. (2025). Multi objective optimization of composite laminate repaired by patches in considering static strength and fatigue life. Mechanics of Advanced Materials and Structures, 32(10): 2322-2342. https://doi.org/10.1080/15376494.2024.2378367

[21] Tan, S.C. (2017). Stress Concentrations in Laminated Composites. Routledge.

[22] Yuan, K., Liu, K., Wang, Z., Yang, M. (2021). An investigation on the perforation resistance of laminated CFRP beam and square plate. International Journal of Impact Engineering, 157: 103967. https://doi.org/10.1016/j.ijimpeng.2021.103967

[23] Rezaeepazhand, J., Jafari, M. (2005). Stress analysis of perforated composite plates. Composite Structures, 71(3-4): 463-468. https://doi.org/10.1016/j.compstruct.2005.09.017

[24] Jafari, M., Rohani, A. (2016). Optimization of perforated composite plates under tensile stress using genetic algorithm. Journal of Composite Materials, 50(20): 2773-2781. https://doi.org/10.1177/0021998315612540

[25] Tsai, C.L., Daniel, I.M., Yaniv, G. (1990). Torsional response of rectangular composite laminates. Journal of Applied Mechanics, 57(2): 383-387. https://doi.org/10.1115/1.2892001

[26] Patil, S.D., Chavan, D.S., Kavade, M.V. (2012). Investigation of composite torsion shaft for static structural analysis using finite element analysis. International Journal of Engineering Research and Technology, 1(7): 1-5. https://doi.org/10.17577/IJERTV1IS7186

[27] Cheng, Z.Q., Liu, H., Tan, W. (2024). Advanced

computational modelling of composite materials. Engineering Fracture Mechanics, 305: 110120. https://doi.org/10.1016/j.engfracmech.2024.110120
[28] Nikbakt, S., Kamarian, S., Shakeri, M. (2018). A review on optimization of composite structures Part I: Laminated composites. Composite Structures, 195: 158-185. https://doi.org/10.1016/j.compstruct.2018.03.063
[29] Chen, Y., Xiao, Z., Yang, Y., Wang, H., Wang, H., Bi, Y. (2025). Multi-objective optimization for impact resistance of composite laminates with non-conventional ply orientations: An integrated finite element and machine learning framework. Thin-Walled Structures, 208: 113687. https://doi.org/10.1016/j.tws.2025.113687
[30] Sarasini, F. (2017). Low-velocity impact behaviour of hybrid composites. In Hybrid Polymer Composite Materials, Woodhead Publishing, pp. 151-168. https://doi.org/10.1016/B978-0-08-100787-7.00007-X
[31] Hashin, Z. (1980). Fatigue failure criteria for unidirectional fiber composites. Journal of Applied Mechanics, 48(4): 846-852. https://doi.org/10.1115/1.3157744
[32] Liu, P.F., Zheng, J.Y. (2010). Recent developments on damage modeling and finite element analysis for composite laminates: A review. Materials and Design, 31(8): 3825-3834. https://doi.org/10.1016/j.matdes.2010.03.031
[33] Sobhani, A., Saeedifar, M., Najafabadi, M.A., et al. (2018). The study of buckling and post-buckling behavior of laminated composites consisting of multiple delaminations using acoustic emission. Thin-Walled Structures, 127: 145-156. https://doi.org/10.1016/j.tws.2018.02.011
[34] Chen, D., Luo, Q., Meng, M., Li, Q., Sun, G. (2019). Low velocity impact behavior of interlayer hybrid composite laminates with carbon/glass/basalt fibers. Composites Part B: Engineering, 176: 107191. https://doi.org/10.1016/j.compositesb.2019.107191
[35] Özaslan, E., Güler, M. A., Yetgin, A., Acar, B. (2019). Stress analysis and strength prediction of composite laminates with two interacting holes. Composite Structures, 221: 110869. https://doi.org/10.1016/j.compstruct.2019.04.041
[36] Wysmulski, P. (2025). Effect of hole diameter on failure load and deformation modes in axially compressed CFRP laminates. Materials, 18(15): 3452. https://doi.org/10.3390/ma18153452
[37] Khan, M.K., Junaedi, H., Alshahrani, H., Wagih, A., Lubineau, G., Sebaey, T.A. (2023). Enhanced open-hole strength and toughness of sandwich carbon-Kevlar woven composite laminates. Polymers, 15(10): 2276. https://doi.org/10.3390/polym15102276
[38] Khechai, A., Layachi, M., Belarbi, M.O., Gohery, S., et al. (2025). An extended Greszczuk's analytical method for stress analysis of unsymmetrical laminated composite plates with a circular hole under axial, biaxial, and shear loads. Structures, 72: 108169. https://doi.org/10.1016/j.istruc.2024.108169
[39] Berthelot, J.M. (2005). Composite Materials: Mechanical Behavior and Structural Analysis. Editions Tec & Doc.
[40] Merhar, M. (2020). Determination of elastic properties of beech plywood by analytical, experimental and numerical methods. Forests, 11(11): 1221. https://doi.org/10.3390/f11111221
[41] Casavola, C., Cazzato, A., Moramarco, V., Pappalettere, C. (2016). Orthotropic mechanical properties of fused deposition modeling parts described by classical laminate theory. Materials and Design, 90: 453-458. https://doi.org/10.1016/j.matdes.2015.11.009
[42] Meng, M., Le, H.R., Rizvi, M.J., Grove, S.M. (2015). 3D FEA modeling of laminated composites in bending and their failure mechanisms. Composite Structures, 119: 693-708. https://doi.org/10.1016/j.compstruct.2014.09.048
[43] Beylergil, B. (2020). Multi-objective optimal design of hybrid composite laminates under eccentric loading. Alexandria Engineering Journal, 59(6): 4969-4983. https://doi.org/10.1016/j.aej.2020.09.015
[44] Hwang, M.Y., Park, J.H., Song, J., Hwang, S.W., Kang, H.H., Lee, H.C. (2023). Enhanced reverse-engineering method for accurately predicting lamina properties in laminated composites via combined static and dynamic finite element simulations. Journal of Composites Science, 7(12): 518. https://doi.org/10.3390/jcs7120518
[45] Khashaba, U.A. (2004). In-plane shear properties of cross-ply composite laminates with different off-axis angles. Composite Structures, 65(2): 167-177. https://doi.org/10.1016/j.compstruct.2003.10.012
[46] Pirkle, M.K., Mallick, P.K. (2025). A numerical study of the effect of hole offset on stress concentrations due to a square hole in a quasi-isotropic composite laminate. Journal of Composites Science, 9(6): 286. https://doi.org/10.3390/jcs9060286
[47] Whitney, J.M., Nuismer, R.J. (1974). Stress fracture criteria for laminated composites containing stress concentrations. Journal of Composite Materials, 8(3): 253-265. https://doi.org/10.1177/002199837400800303
[48] Lekhnitskii, S.G. (1981). Theory of Elasticity of an Anisotropic Body. Mir Publishers.
[49] Wang, X., Cai, D.A., Silberschmidt, V.V., Deng, J., Tian, H., Zhou, G. (2019). Tensile properties of 3D multi-layer wrapping braided composite: Progressive damage analysis. Composites Part B: Engineering, 176: 107334. https://doi.org/10.1016/j.compositesb.2019.107334
[50] Beylergil, B., Cunedioğlu, Y., Aktas, A. (2011). Experimental and numerical analysis of single lap composite joints with inter-adherend fibers. Composites Part B: Engineering, 42(7): 1885-1896. https://doi.org/10.1016/j.compositesb.2011.06.010
[51] Zhang, W., Tang, W.Y., Pu, Y.C., Zhang, S.K. (2011). Ultimate strength analysis of ship hulls of continuous basalt fiber composite materials. Advanced Materials Research, 150: 736-740. https://doi.org/10.4028/www.scientific.net/AMR.150-151.736
[52] Zhao, S.Y., Xue, P. (2014). New two-dimensional polynomial failure criteria for composite materials. Advances in Materials Science and Engineering, 2014(1): 503483. https://doi.org/10.1155/2014/503483
[53] Shokrieh, M.M., Lessard, L.B. (2000). Progressive fatigue damage modeling of composite materials, Part II: Material characterization and model verification. Journal of Composite Materials, 34(13): 1081-1116. https://doi.org/10.1177/002199830003401302
[54] ANSYS Inc. (2015). ANSYS User's Manual, Version 16.2.
[55] Deb, K. (2001). Multi-Objective Optimization using Evolutionary Algorithms. John Wiley & Sons Ltd.

[56] Lee, D.S., Morillo, C., Bugeda, G., Oller, S., Onate, E. (2012). Multilayered composite structure design optimization using distributed/parallel multi-objective evolutionary algorithms. Composite Structures, 94(8): 2641-2653. https://doi.org/10.1016/j.compstruct.2011.10.009

[57] Anam, S. (2019). Parameters estimation of enzymatic reaction model for biodiesel synthesis by using real coded genetic algorithm with some crossover operations. IOP Conference Series: Materials Science and Engineering, 546: 052006. https://doi.org/10.1088/1757-899X/546/5/052006

[58] Albadr, M.A., Tiun, S., Ayob, M., Al-Dhief, F. (2020). Genetic algorithm based on natural selection theory for optimization problems. Symmetry, 12(11): 1758. https://doi.org/10.3390/sym12111758

[59] Zhang, Z., Liao, C., Chai, H., Ni, X., et al. (2021). Multi-objective optimization of controllable configurations for bistable laminates using NSGA-II. Composite Structures, 266: 113764. https://doi.org/10.1016/j.compstruct.2021.113764

[60] Verma, S., Pant, M., Snasel, V. (2021). A comprehensive review on NSGA-II for multi-objective combinatorial optimization problems. IEEE Access, 9: 57757-57791. https://doi.org/10.1109/ACCESS.2021.3070634

[61] Chakraborti, N., Sreevathsan, R., Jayakanth, R., Bhattacharya, B. (2009). Tailor-made material design: A evolutionary approach using multi-objective genetic algorithms. Computational Materials Science, 45(1): 1-7. https://doi.org/10.1016/j.commatsci.2008.03.054

[62] Khireddine, B., Samir, G.M., Djamel, H. (2025). A multi-objective optimization of window surface and glass thickness determination for daylight factor, thermal resistance and acoustic insulation of a test room performances under an overcast sky. Journal of Building Engineering, 101: 111717. https://doi.org/10.1016/j.jobe.2024.111717

[63] Yoshino, Y., Kimura, Y. (2024). Rotational stiffening performance of roof folded plates in torsion tests and the stiffening effect of roof folded plates on the lateral buckling of H beams in steel structures. Buildings, 14(4): 1158. https://doi.org/10.3390/buildings14041158

[64] Nikopour, H., Selvadurai, A.P.S. (2013). Torsion of a layered composite strip. Composite Structures, 95: 1-4. https://doi.org/10.1016/j.compstruct.2012.08.027

[65] Jule, L.T., Ramaswamy, K., Nagaprasad, N., Shanmugam, V., Vignesh, V. (2021). Design and analysis of serial drilled hole in composite material. Materials Today: Proceedings, 45: 5759-5763. https://doi.org/10.1016/j.matpr.2021.02.587